

# Chiral tunneling in single layer graphene with Rashba spin-orbit coupling: spin currents

Y. Avishai<sup>1</sup> and Y. B. Band<sup>2</sup>

<sup>1</sup>*Department of Physics, Ben-Gurion University of the Negev, Beer-Sheva, Israel, New York University and the NYU-ECNU Institute of Physics at NYU Shanghai, 3663 Zhongshan Road North, Shanghai, 200062, China, and Yukawa Institute for Theoretical Physics, Kyoto, Japan*

<sup>2</sup>*Department of Physics, Department of Chemistry, Department of Electro-Optics, and The Ilse Katz Center for Nano-Science, Ben-Gurion University of the Negev,*

We study forward scattering of 2D massless Dirac electrons at Fermi energy  $\varepsilon > 0$  in single layer graphene through a 1D rectangular barrier of height  $u_0$  in the presence of uniform Rashba spin-orbit coupling (of strength  $\lambda$ ). The role of the Klein paradox in graphene spintronics is thereby exposed. It is shown that (1) For  $\varepsilon - 2\lambda < u_0 < \varepsilon + 2\lambda$  there is partial Klein tunneling, wherein the transmission is bounded by 1 and, quite remarkably, for small  $\lambda > \lambda_0 \approx 0.1$  meV, the transmission nearly vanishes when the scattering energy equals the barrier height,  $\varepsilon = u_0$ . (2) Spin density and spin-current density are shown to be remarkably different than these observables predicted in bulk single layer graphene. In particular, they are sensitive to  $\lambda$  and  $u_0$ . (3) Spin current densities are space dependent, implying the occurrence of non-zero spin torque density. Such a system may serve as a graphene based spintronic device without the use of an external magnetic field or magnetic materials.

*Introduction:* Shortly after the discovery of graphene [1], numerous novel physical phenomena were revealed in its electronic properties [2, 3]. One of these, the occurrence of chiral tunneling and the Klein paradox [4] in single layer graphene (SLG), was reported in a seminal paper [5]. This work was further expanded in Refs. [6–8]. It was shown that, due to chirality near a Dirac point, electrons execute unimpeded transmission for energies below the potential barrier. This phenomenon is related to the absence of back-scattering for electron-impurity scattering in carbon nanotubes [9]. Several additional extensions have been reported in Refs. [10–12]. In parallel, investigation of the role of electron spin in graphene led to the emergence of a new field: graphene spintronics [13–56].

Here we study Klein tunneling of 2D massless Dirac electrons at Fermi energy  $\varepsilon > 0$  in SLG, through a 1D barrier of height  $u_0$  in the presence of uniform RSOC of strength  $\lambda$  [57]. The motivation is to elucidate the effect of the Klein paradox on observables such as spin density, spin current density and spin torque [58]. It is shown that the calculated spin observables have properties that are remarkably different from those predicted in bulk SLG [48] (i.e., in the absence of a 1D potential so that the Klein paradox does not play a role). In particular, some symmetry relations are broken (see below), and the spin current is space dependent so that there is a finite spin torque. But most importantly, the response of the spin densities to the RSOC strength is substantial even for small RSOC coupling (the strength of Rashba splitting caused by a strong electric field in SLG is reported in Ref. [45] to be a fraction of an meV). This leads us to hope that our study will motivate the fabrication of graphene based spintronic devices that do not rely on the use of an external magnetic field or magnetic materials. We also expose an intriguing behavior of the transmission coefficient  $T(\varepsilon, \lambda, u_0)$ : In the (very narrow) region  $\varepsilon - 2\lambda < u_0 < \varepsilon + 2\lambda$  only one scattering channel is open, and the transmission in the forward direction is bounded by 1 (for  $\lambda = 0$ ,  $T = 2$ ). Moreover, for scattering energy equal to the barrier height,  $\varepsilon = u_0$ , one channel is about to open and the second channel is about to close, and the transmission coefficient almost vanishes. In what follows, we will (1) present the formalism used, (2) explain the choice of parameters (3) analyze the properties of the transmission, (4) derive expressions for spin density and spin current density, (5) present results and (6) conclude with a short summary.

*Formalism:* We formulate the problem of massless 2D Dirac electrons in SLG lying in the  $x$ - $y$  plane that are scattered from a 1D rectangular potential barrier of  $u(x) = u_0\Theta(x)\Theta(d - x)$  and subject to a uniform electric field  $\mathbf{E} = E_0\hat{\mathbf{z}}$ . Our treatment is carried out within the continuum formulation near one of the Dirac points, say  $\mathbf{K}'$ . Since the transverse wave number  $k_y$  is conserved, the wave function can be factored:  $\Psi(x, y) = e^{ik_y y}\psi(x)$ . Recall that, in addition to the isospin  $\boldsymbol{\tau}$  encoding the two-lattice structure of graphene, there is now a *real spin*,  $\boldsymbol{\sigma}$ . Hence, the wave function  $\psi(x)$  is a four component vector in  $\boldsymbol{\sigma} \otimes \boldsymbol{\tau}$  (spin $\otimes$ isospin) space.  $\psi(x)$  has dimensions of  $1/\sqrt{A}$  where  $A$  is some relevant area (hereafter,  $A = 1$  (nm) $^2$ , is omitted when no confusion arises). In our calculations we make use of units such that  $\hbar v_F = 1$  ( $v_F = 10^8$  cm/sec is the Fermi velocity). Hence, lengths are given in nm, while wave numbers  $k_x, k_y, q_x, q_y$ , energies  $\varepsilon, u_0$  and RSOC strength  $\lambda$  are given in (nm) $^{-1}$ . In particular,  $\lambda \propto 1/\ell_{so} \propto E_0$ , where  $\ell_{so}$  is the spin-orbit length [59]. However, in presenting our numerical results, energies  $\varepsilon, u_0$  and RSOC strength  $\lambda$  will be presented in meV, [1 (nm) $^{-1} = 659.107$  meV]. The Hamiltonian for the scattering problem is given by

$$\begin{aligned} h(-i\partial_x, k_y, \lambda) &= [-i\partial_x + \lambda(\hat{\mathbf{z}} \times \boldsymbol{\sigma})_x]\tau_x \\ &+ [k_y + \lambda(\hat{\mathbf{z}} \times \boldsymbol{\sigma})_y]\tau_y + u(x) \\ &\equiv h_0(-i\partial_x, k_y, \lambda) + u(x). \end{aligned} \quad (1)$$

which is a  $4 \times 4$  matrix first-order differential operator acting on the four component vector  $\psi(x)$ . The latter is a combination of plane-wave vectors,  $e^{\pm ik_x x}u(\pm k_x)$  ( $x \notin [0, d]$ ), and  $e^{\pm iq_x x}w(\pm q_x)$  ( $x \in [0, d]$ ). The normalized 4 component vectors  $u(\pm k_x)$  and  $w(\pm q_x)$  satisfy the equations,

$$\begin{aligned} h_0(\pm k_x, k_y, \lambda)u(\pm k_x) &= \varepsilon u(\pm k_x), \\ h(\pm q_x, k_y, \lambda)w(\pm k_x) &= \varepsilon w(\pm k_x), \end{aligned} \quad (2)$$

where  $\varepsilon$  is the scattering (Fermi) energy. Because RSOC acts in all of space, (not only in the barrier region), the vectors  $u(\pm k_x)$  cannot be chosen as spin eigenfunctions *since spin is not conserved*. Moreover, Eqs. (3) are not eigenvalue equations. Indeed, assuming fixed transverse wave number  $k_y$ , potential parameters  $u_0, d$  and RSOC strength  $\lambda$ , the wave numbers  $k_x$  and  $q_x$  must depend on the (already fixed) scattering energy  $\varepsilon$ . Equations (3) are implicit equations for  $k_x(\varepsilon), q_x(\varepsilon)$  as well as for  $u[\pm k_x(\varepsilon)]$  and  $w[\pm q_x(\varepsilon)]$ . For  $\varepsilon > 0$ , there are two wave numbers in each region that solve these implicit equations,  $\pm k_{xn}(\varepsilon)$  for  $x \notin [0, d]$ , and  $\pm q_{xn}(\varepsilon)$

for  $x \in [0, d]$  ( $n=1,2$ ). Solution of Eqs. (2) yields

$$\begin{aligned} k_{xn}^2 &= [\varepsilon^2 + (-1)^{n+1}\lambda]^2 - \lambda^2 - k_y^2, \\ q_{xn}^2 &= [\varepsilon^2 + (-1)^{n+1}\lambda - u_0]^2 - \lambda^2 - k_y^2, \end{aligned} \quad (3)$$

together with the vectors  $u_n(\pm k_{xn})$  and  $w_n(\pm q_{xn})$ . This leads to a *two-channel scattering problem*. Recall that in the absence of RSOC, where there is a single channel, the Klein paradox occurs for  $u_0 > \varepsilon > 0$ , and the single wave number  $q_x = \sqrt{(u_0 - \varepsilon)^2 - k_y^2}$  is always real in the forward direction  $k_y = 0$ , which implies unimpeded transmission. When  $\lambda > 0$  the wave numbers  $q_{xn}$  can be complex. As we shall see below, there is a region in which there is partial Klein tunneling. The wave function corresponding to an incoming wave in channel  $n$  ( $n = 1, 2$ ) in the three regions is,

$$\psi_n(x) = \begin{cases} \underbrace{|k_{xn}\rangle + r_{n1}|\bar{k}_{x1}\rangle + r_{n2}|\bar{k}_{x2}\rangle}_{x < 0} \\ \underbrace{a_{n1}^+|q_{x1}\rangle + a_{n2}^+|q_{x2}\rangle + a_{n1}^-|\bar{q}_{x1}\rangle + a_{n2}^-|\bar{q}_{x2}\rangle}_{0 < x < d} \\ \underbrace{t_{n1}|k_{x1}\rangle + t_{n2}|k_{x2}\rangle}_{x > d} \end{cases} \quad (4)$$

$$|k_{xn}\rangle \equiv e^{ik_{xn}x}u_n(k_{xn}), \bar{k}_{xn} \equiv -k_{xn},$$

$$|q_{xn}\rangle \equiv e^{iq_{xn}x}w_n(q_{xn}), \bar{q}_{xn} \equiv -q_{xn}.$$

The matching conditions at  $x = 0$  and  $x = d$  yield the transmission and reflection amplitude matrices  $t = (t_{11} t_{12})$  and  $r = (r_{11} r_{12})$  together with the eight coefficients  $\{a_{nm}^\pm\}$ , ( $n, m = 1, 2$ ). The wave functions  $\psi_n(x)$  with scattering boundary conditions are therefore determined everywhere. The solution obeys unitarity and charge current conservation,

$$\begin{aligned} T + R &= \text{Tr}[t^\dagger t] + \text{Tr}[r^\dagger r] = 2, \\ \frac{d}{dx}j(x) &\equiv \frac{d}{dx} \sum_{n=1}^2 \psi_n^\dagger(x) \hat{j}_x \psi_n(x) = 0. \end{aligned} \quad (5)$$

$T$  and  $R$  are the transmission and reflection coefficients and  $\hat{j}_x = I_2 \otimes \tau_x$  is the current operator.

*Choice of parameters:* Our objective is to explore the response of the system to variation of the RSOC strength  $\lambda$  (tunable by the electric field), the scattering energy  $\varepsilon$  and the potential parameters  $u_0, d$  (tunable by gate voltage). For simplicity, we consider forward scattering,  $k_y = 0$  (the case  $k_y \neq 0$  will be explored in a future communication). Note that it is experimentally difficult to tune  $k_y$  for fixed Fermi energy  $\varepsilon$ . The numerical choice of parameters is dictated by experiments. In Ref. [45], it is shown that for a field  $E_R = 2$  V/nm,  $\lambda$  is on the order of a fraction of an meV. Here we let  $0 < \lambda \leq 0.65$  meV, and vary the barrier height in the range  $0 < u_0 < 200$ . The barrier width  $d$  is taken at 200 nm (except for Fig. 1 where  $d = 60$  nm). Next, in the absence of RSOC, the Klein paradox emerges for  $u_0 > \varepsilon > 0$  (the Fermi energy outside the barrier is in the conduction band and inside the barrier it is in the valence band). In the presence of RSOC, this condition is slightly modified as follows: For each  $u_0 > 0$ , at least one of the wave numbers  $\{q_{xn}\}$  is real [see Eq. (3)]. For  $k_y = 0$ , this implies  $u_0 > \varepsilon - 2\lambda > 0$  [see Fig. 1(a)]. Concerning the choice of  $\varepsilon$ , it is expected that the interesting physics occurs for  $\varepsilon$  close to  $\lambda$ . These considerations are highlighted in Fig. 1(b). Practically, since  $\varepsilon, \lambda \approx$  a few meV, for a barrier height of  $u_0 \approx 100\text{-}300$  meV, both momenta  $\{q_{xn}\}$  are real.

*Transmission:* For  $k_y = 0$ , the two channels are uncoupled, and the transmission coefficient is ob-

tained analytically:

$$T(u_0; \varepsilon, \lambda, ky = 0) = \sum_{n=1}^2 \frac{q_{xn}^2}{(u_0 - \varepsilon)[(u_0 - \varepsilon) + 4\lambda] - \lambda^2 \sin^2(q_{xn}d)}. \quad (6)$$

Partial Klein tunneling occurs if one of the squared wave numbers, say  $q_{x2}^2$ , is negative. The second term ( $n = 2$ ) in Eq. (6) still remains real and non-negative, because  $-\sin^2(q_{x2}d) = \sinh^2(|q_{x2}|d) > 0$ . Practically, however, for  $|q_{x2}|d \gg 1$  the denominator is so large that the contribution of this term to the transmission is minuscule, and channel 2 is virtually closed. Thus, Klein paradox is still manifest even if only one channel is open. That happens if  $0 < \varepsilon - 2\lambda < u_0 < \varepsilon + 2\lambda$ , (and then  $T \leq 1$ ). A single channel scattering occurs for  $\varepsilon - 2\lambda < u_0 < \varepsilon$  [blue curve in Fig. 1(a) and panel 2 in Fig. 1(b)], or for  $\varepsilon < u_0 < \varepsilon + 2\lambda$  [red curve in Fig. 1(a) and panel 4 in Fig. 1(b)]. For  $\varepsilon + 2\lambda < u_0$ ,  $q_{xn}^2 > 0$  [panel 5 in Fig. 1(b)], and  $1 < T \leq 2$ . Inspecting  $T(u_0; \varepsilon, \lambda, ky = 0)$  as function of  $u_0$  in Fig. 1(c), shows that when the scattering energy equals the barrier height,  $\varepsilon = u_0$  [panel 3 in Fig 1(b)],  $T(u_0; \varepsilon = u_0, \lambda, ky = 0) \approx 0$ . Recall from Eq. (6) that for  $\lambda = 0$  the transmission is unimpeded,  $T(u_0; \varepsilon, \lambda = 0, ky = 0) = 2$  (identically). But the inset in Fig. 1(c) shows that this happens for very small  $\lambda$ . Note that in the corresponding 1D Schrödinger problem for  $\varepsilon = u_0$ ,  $T = \frac{4}{4 + (kd)^2}$  where  $k = \sqrt{\frac{2m\varepsilon}{\hbar^2}}$ . Therefore, a pertinent experiment for  $\lambda \neq 0$  should be an excellent probe of the strength of RSOC in SLG.

We now consider the transmission coefficient  $T$  and the charge current  $j(x)$  as a function of potential barrier height parameter  $u_0 > \varepsilon + 2\lambda$  and the RSOC strength parameter  $\lambda$ . Figure 2(a) shows the transmission and current versus  $\lambda$  for fixed  $u_0$  and Fig. 2(b) shows the transmission and current versus  $u_0$  for fixed  $\lambda$ . The main conclusion from these figures is that in the presence of RSOC, the transmission coefficient is no longer unimpeded. Rather, for fixed  $u_0$  and for experimentally relevant interval  $0 < \lambda < 0.65$  meV it smoothly decreases as in Fig. 1(a). Moreover, for fixed  $\lambda$ , considered as function of the barrier height  $u_0$  it possess a beautiful pattern of oscillations below the unitarity upper limit  $T = 2$  as shown in Fig. 2(b). It is of course not surprising that the charge current and the transmission coefficient are highly correlated. Note that the charge current is space-independent [see Eq. (5)].

*Spin density:* Spin density (and spin current density) operators  $\{\mathcal{O}\}$  are representable as  $4 \times 4$  matrices in  $\boldsymbol{\sigma} \otimes \boldsymbol{\tau}$  space. Spin observables are obtained as  $O(x) = \psi^\dagger(x) \mathcal{O} \psi(x)$  (this is not an expectation value, spin-observables may depend on  $x$ ). The spin density operators  $\hat{\mathbf{S}}$  and the spin density observables  $\mathbf{S}(x)$  are given by,

$$\begin{aligned} \hat{\mathbf{S}} &= (\hat{S}_x, \hat{S}_y, \hat{S}_z) = \frac{1}{2} \hbar \boldsymbol{\sigma} \otimes \mathbf{I}_2, \\ \mathbf{S}(x) &= \frac{1}{2} \sum_{n=1}^2 \psi_n^\dagger(x) \hat{\mathbf{S}} \psi_n(x), \end{aligned} \quad (7)$$

where  $\psi_n(x)$  is defined in Eq. (4). The unit of spin density used here is  $S_0 = \hbar/A$ . Of the three spin density observables, two of them vanish,  $S_x = S_z = 0$ , i.e., there is no polarization neither along the direction of motion nor in a direction perpendicular to the SLG plane. This is consistent with the results of Ref. [48] wherein the spin density distribution is calculated in bulk SLG [for  $k_y = 0$  and  $\sin \theta = 0$ , see Eq. (5) therein]. Figure 3(a) shows the spin density

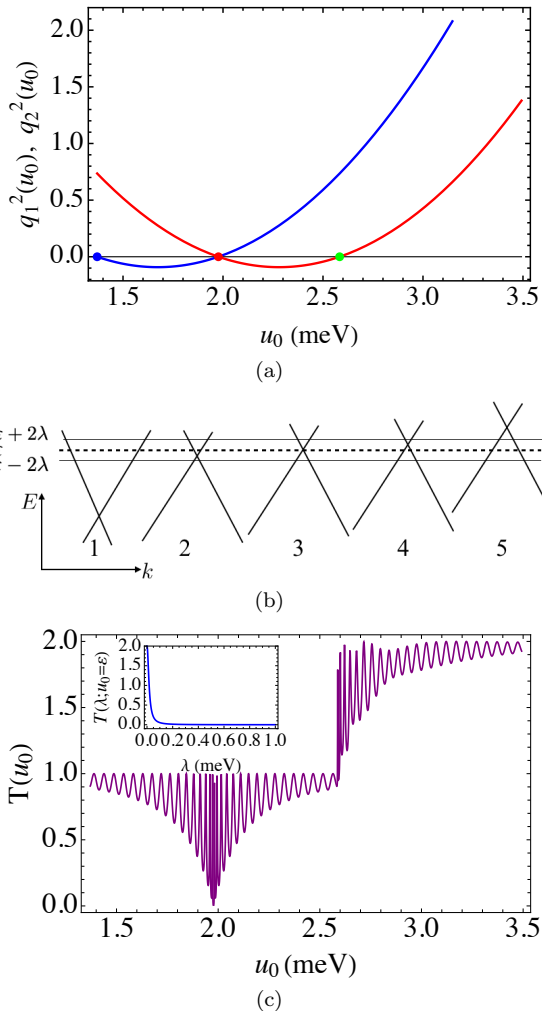


FIG. 1. Partial Klein transmission through a barrier of small height  $u_0$ , occurs when  $|u_0 - \varepsilon| < 2\lambda$ . Here we take  $\varepsilon = 1.977$  meV,  $\lambda = 0.30314$  meV, and barrier width  $d = 60$  nm. (a) Squared wavenumbers,  $q_{xn}^2$  defined in Eq. (3) (blue for  $n = 1$  and red for  $n = 2$ ). The blue, green and red points mark  $u_0 = (\varepsilon - 2\lambda, \varepsilon, \varepsilon + 2\lambda)$ . Negative  $q_{xn}^2$  implies that channel  $n$  is closed (does not contribute to the transmission). (b) Dirac cones for various values of  $u_0$  (schematic), Fermi energy  $\varepsilon$  and SO splitting  $\varepsilon \pm 2\lambda$  (magnified): In panels 1-5,  $u_0 = 0, \varepsilon - \lambda, \varepsilon, \varepsilon + \lambda$  and  $u_0 > \varepsilon + 2\lambda$ . (c) Total transmission is plotted versus  $u_0$  for  $\varepsilon - 2\lambda < u_0 < 3.5$  (meV). A remarkable feature of RSOC is that for  $u_0 \approx \varepsilon$  (red point in (a) where one channel is about to open and the other is about to close), the transmission nearly vanishes except for  $\lambda \rightarrow 0$  where, as shown in the inset, it sharply rises to 2 [see Eq. (6)].

$S_y(x = 0)$  just outside the left wall of the barrier of the p-n-p junction as a function of  $\lambda$  [note however, that the spin densities are space-independent,  $S_y(x) = S_y(0)$ ]. The size of the polarization substantially increases for  $\lambda > 0.20$  meV. Figure 3(b) plots  $S_y$  versus  $u_0$ , and shows a rich oscillatory pattern that decreases near the lower limit  $u_0 = \varepsilon + 2\lambda$ , below which one channel is closed (see discussion of Fig. 1). Both parts of Fig. 3 substantiate the role of the RSOC strength and the barrier height as useful parameters to control the degree of polarization.

*Spin current density operators and observables:* The (tensor) spin-current density operator  $\hat{\mathbb{J}}$  and the observed components of the spin current density  $J_{ij}(x)$  are defined as

$$\hat{\mathbb{J}} = \frac{1}{2}\{\hat{\mathbf{S}}, \hat{\mathbf{V}}\}, \Rightarrow \hat{\mathbb{J}}_{i,j} = \hat{S}_i \hat{V}_j + \hat{V}_j \hat{S}_i, \\ J_{ij}(x) = \frac{1}{2} \sum_{n=1}^2 \psi_n^\dagger(x) \hat{\mathbb{J}}_{ij} \psi_n(x), \quad (8)$$

where  $\hat{\mathbf{S}}$  is the spin density operator defined in Eq. (7) and  $\hat{\mathbf{V}} = \mathbf{I}_2 \otimes \boldsymbol{\tau}$  is the velocity operator [equal the charge current operator  $\hat{j}_x$  defined in Eq. (5)]. In Eq. (8),  $i = 1, 2, 3 = x, y, z$  specifies the polarization direction, and  $j = 1, 2 = x, y$  specifies the axis along which electrons propagate. The

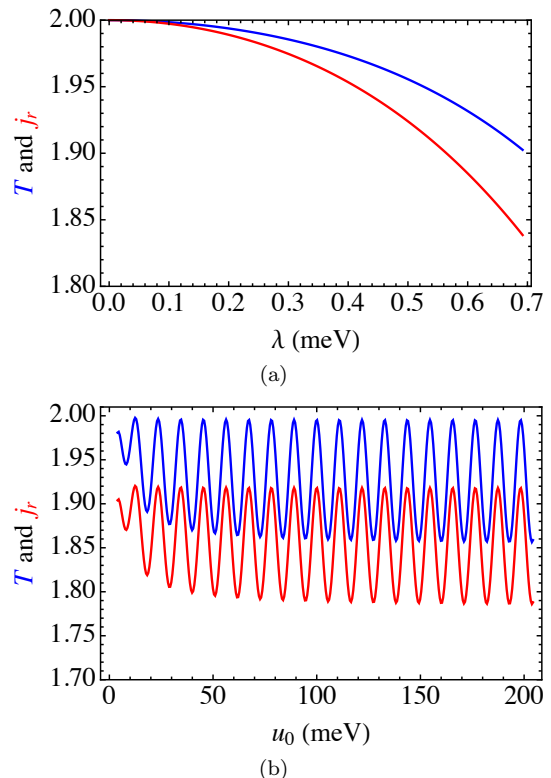


FIG. 2. Transmission  $T$  (blue) and charge current  $j_r$  (red) for the p-n-p junction. The current was calculated on the right wall of the barrier but its divergence vanishes, as required by Eq. (5), hence it is space-independent. (a) Transmission and current versus  $\lambda$  for  $u_0 = 195$  meV,  $d = 200$  nm,  $\varepsilon = 6.65$  meV and  $k_y = 0$  (whereas for  $\lambda = 0$ ,  $T(k_y = 0) = 2$ , and  $\lambda > 0$ ,  $T(k_y = 0) < 2$ ). (b) Transmission and current versus  $\varepsilon + 2\lambda < u_0 < 200$  meV for  $\lambda = 0.695$  meV [other parameters as in (a)].

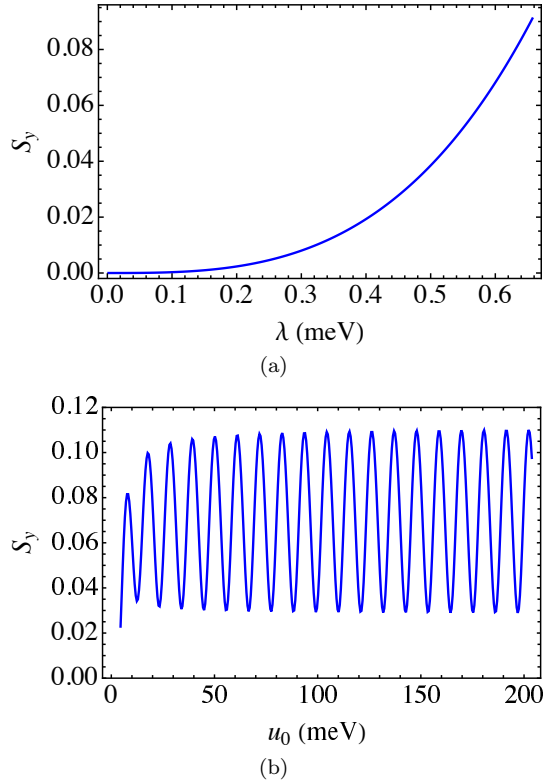


FIG. 3. (a) Spin density  $S_y$  as function of  $\lambda$  for  $u_0 = 192$  meV,  $d = 200$  nm,  $\varepsilon = 2.60$  meV and  $k_y = 0$ . (b)  $S_y$  versus  $\varepsilon + 2\lambda < u_0 < 200$  meV for  $\lambda = 0.695$  meV and  $k_y = 0$  [other parameters are as in (a)]. Note that  $S_y(x)$  is independent of  $x$  throughout the sample.

unit of spin current density is  $J_0 = S_0 v_F = \gamma/A = 659.107$  meV/nm.

The spin current density was calculated in bulk SLG in Ref. [48]; it was found that (1)  $J_{xx} = J_{yy} = J_{zx} = J_{zy} = 0$ , (2)  $J_{xy} = -J_{yx}$ , and (3) The spin currents are independent on space [see Eq. (5) in Ref. [48]]. Below, we show that: (1) In the presence of a 1D potential (where there is no rotational symmetry around the  $z$ -axis), the symmetry rela-

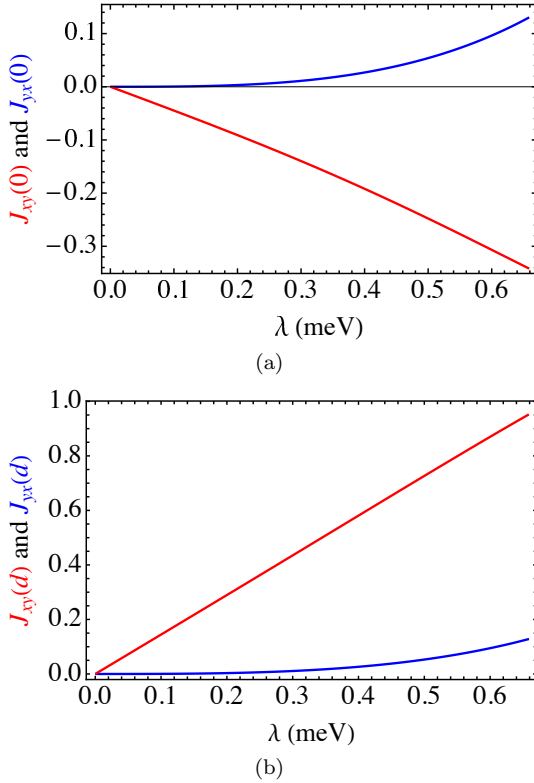


FIG. 4. Spin current density (in units of  $J_0$ ) at the left ( $x = 0$ ) and right ( $x = d$ ) barrier walls versus  $\lambda$  for  $u_0 = 192$  meV,  $d = 200$  nm,  $\varepsilon = 2.60$  meV. (a) Spin current densities  $J_{yx}(x = 0)$  (blue) and  $J_{xy}(x = 0)$  (red). (b)  $J_{yx}(x = d)$  (blue) and  $J_{xy}(x = d)$  (blue) versus  $\lambda$ . Note that the symmetry condition  $J_{xy} = -J_{yx}$  valid in bulk SLG [48] is broken by the 1D potential barrier.

tion  $J_{xy} = -J_{yx}$  that is valid in bulk SLG [48] is broken. (2) Although the value of  $\lambda$  used in our calculations is much smaller than that used in Ref. [48], the size of spin current densities are both systems is the same. (3) The divergence of the spin current does not vanish, and hence the continuity equation for the spin current density must contain a spin torque density term [58]. Figure 4(a) (red curve) shows the spin current densities  $J_{xy}(0)$  (red curve) and  $J_{yx}(0)$  (blue curve), just at the left wall of the barrier, for the p-n-p junction as function of  $\lambda$ . The size of the spin current density  $J_{xy}(0)$  (electrons polarized along  $x$  and propagate along  $y$ ) for  $\lambda \approx 0.659$  meV is indeed large (as compared with  $J_{xy}$  in bulk SLG calculated for  $\lambda \approx 45$  meV). Figure 4(b) shows  $J_{xy}(d)$  and  $J_{yx}(d)$  as function of  $\lambda$ . The nearly linear increase of  $J_{xy}(0)$  and  $J_{xy}(d)$  with  $\lambda$  is an encouraging feature in the quest for exposing novel and practical aspects graphene spintronics. No symmetry exists between  $J_{xy}$  and  $J_{yx}$ .

To stress the role of the Klein paradox in the present system we compare our results with those obtained in bulk SLG (where there is no Klein paradox). In Eq. (7) of Ref. [48], the authors found that in bulk SLG,  $J_{yx} = J_0 \frac{\eta^2 + \cos 2\phi}{1 + \eta^2}$  where  $\eta = \frac{\varepsilon}{\sqrt{k_x^2 + k_y^2}}$  is of order unity and  $\phi = \arctan k_y/k_x$ . Thus, for  $k_y = 0$ , this implies  $J_{yx} = -J_{xy} \approx J_0$ . As shown in Figs. 4, 5 and 6, in the presence of 1D potential barrier, the spin current density can reach similar values. However, in Ref. [48] the value of  $\lambda$  is about 200 times higher than the one we have used. As shown in Ref. [45], such high values of  $\lambda$  are not achievable in SLG. It is possible to have higher values of RSOC if the SLG is in contact with metals such as Au or Pb. But upon passing a current through the metallic substrate, the electrons will flow through the metal and not through the SLG, so at the Fermi level, the electronic states are metallic.

Spin current densities versus potential height  $u_0$  are shown in Fig. 5. Recalling the behavior of  $S_y(u_0)$  shown in Fig. 3(b), and of  $J_{xy}(u_0)$  and

$J_{yx}(u_0)$  in Fig. 5, it is clear that the spin density and the spin current density are significantly correlated.

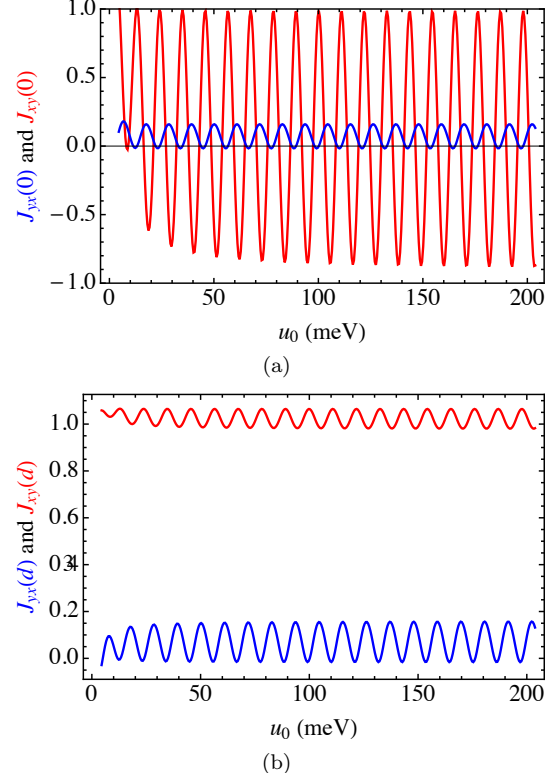


FIG. 5. (a) Spin current densities  $J_{xy}(x)$ ,  $J_{yx}(x)$  on the left and right walls of the barrier versus  $\lambda$  for  $\varepsilon + 2\lambda < u_0 < 200$  meV,  $d = 200$  nm,  $\varepsilon = 2.60$  meV,  $\lambda = 0.695$  meV and  $k_y = 0$ . (a) On the left wall,  $x = 0$ , and (b) On the left wall  $x = d$ .

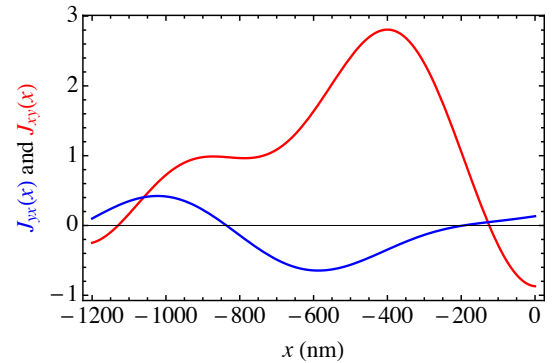


FIG. 6. Space dependence of the spin current densities  $J_{xy}(x)$  and  $J_{yx}(x)$  (in units of  $J_0$ ) for  $-1200 < x < 0$  nm (region to the left of the barrier, where the wave is reflected) for  $\lambda = 0.695$  meV,  $\varepsilon = 2.60$  meV, and  $u_0 = 198.2$  meV. The oscillatory structure due to the linear combination of plane waves continues to  $x \rightarrow -\infty$ .

An important result of the present study concerns the space dependence of the spin current density (recall that the spin density  $\mathbf{S}$  is space-independent). The spin current densities  $J_{xy}(x)$  and  $J_{yx}(x)$  are plotted in Fig. 6 to the left of the barrier (the reflected region) where the wave numbers  $k_{xn}$  [defined in the first row of Eq. (3)], are small (since  $\varepsilon$  and  $\lambda$  are small). Space dependence means non-zero divergence, and the corresponding continuity equation requires the inclusion of finite spin torque density [58]. In the general case, one considers a 3D material wherein the observable spin current density tensor  $\mathbf{J}_{ij}(\mathbf{r})$  depends on the position vector  $\mathbf{r}$ . For each polarization direction  $i = x, y, z$  the vector field  $\mathbf{J}_i(\mathbf{r}) = (J_{ix}(\mathbf{r}), J_{iy}(\mathbf{r}), J_{iz}(\mathbf{r}))$  satisfies the continuity equation,

$$\frac{\partial}{\partial t} S_i + \nabla \cdot \mathbf{J}_i(\mathbf{r}) = \mathcal{T}_i(\mathbf{r}) \equiv \text{Re}[\psi^\dagger(\mathbf{r}) \hat{T}_i \psi(\mathbf{r})]. \quad (9)$$

Here the scalar  $\mathcal{T}_i(\mathbf{r})$  is the spin torque density and  $\hat{T}_i = \frac{1}{i\hbar} [\hat{S}_i, H]$  is the spin torque density operator,

where  $H = (\mathbf{p} + \lambda\boldsymbol{\sigma} \times \mathbf{n}_E) \cdot \boldsymbol{\tau}$  is the Hamiltonian operator and  $\mathbf{n}_E$  is the unit vector in the direction of the electric field. The volume integral of  $\mathcal{T}_i(\mathbf{r})$  sometimes vanishes due to symmetry relations [58], and then there exists a vector field  $\mathbf{P}_i(\mathbf{r})$  such that  $\mathcal{T}_i(\mathbf{r}) = -\nabla \cdot \mathbf{P}_i(\mathbf{r})$ . In 1D, the continuity equation is  $\frac{\partial}{\partial t} S_i + [\frac{dJ_i(x)}{dx} + P_i(x)] = 0$ . In the static case, this gives  $\mathcal{T}_i(x) = \frac{dJ_i(x)}{dx}$ . The two vector fields are  $\mathbf{J}_1(x) = (0, J_{xy}(x))$  and  $\mathbf{J}_2(x) = (J_{yx}(x), 0)$ . Therefore, the only non-zero spin torque density is  $\mathcal{T}_2(x) = dJ_{yx}(x)/dx$ . As we saw in Fig. 6, in the region  $x < 0$ ,  $J_{yx}(x)$  is very smooth, and the spin torque density is well defined (and hopefully measurable).

*Summary and Conclusion:* The Klein paradox in SLG occurs at the Fermi energy  $\varepsilon$  when an electron tunnels through a 1D potential barrier of height  $u_0$  (which can be experimentally controlled by a gate voltage) in the region  $u_0 > \varepsilon > 0$ . When, in addition, a uniform perpendicular electric field  $\mathbf{E} = E_0\hat{\mathbf{z}}$  is applied, the role of electron spin enters due to RSOC. Here we elucidate the physics when the Klein paradox and RSOC are combined, in order to expose interesting facets of graphene spintronics within a time-reversal invariant formalism. The fact that  $u_0$  and  $\lambda$  can be easily experimentally controlled makes our analysis readily verifiable. This combination implies a very small transmission for low barrier at energy equal to the barrier height  $\varepsilon = u_0$  [Fig. 1(c)], while for high barrier it decreases smoothly as function  $\lambda$  [Fig. 2(a)], and

oscillates as function of  $u_0$  [Fig. 2(b)] (recall that in the absence of RSOC, the transmission in the forward direction  $k_y = 0$  is constant at its maximum possible value,  $T = 2$ ). Spin observables are calculated and their behavior as a function of  $\lambda$ ,  $u_0$  and position are presented. The only non-zero spin density is  $S_y$  (shown in Figs. 3(a) and 3(b)).  $S_y$  is independent of  $x$ . Spin current density  $J_{ij}$  is plotted as a function of  $\lambda$  in Fig. 4; the magnitude of  $J_{yx}$  increases linearly with  $\lambda$ . In Fig. 5, the spin current density is plotted versus  $u_0$  and shows sharp oscillations. It is evident that the symmetry  $J_{xy} = -J_{yx}$  derived in pure SLG [48] is broken here. The spin current density is plotted versus  $x$  in Fig. 6. Clearly, the present system (compared with bulk SLG),  $J_{ij}(x)$  has a much richer pattern and non-trivial space dependence (associated with non-zero spin torque density [58]).

Following the resent developments in spintronics in general [60–64], our work was partially motivated by the quest for constructing spintronic devices without the use of an external magnetic field or magnetic materials. We hope that our results, pertaining to graphene, such as the nearly linear dependence of the spin current density  $J_{xy}(d)$  on  $\lambda$ , and the vanishing transmission at energy  $\varepsilon = u_0$ , advance this goal.

*Acknowledgement:* Discussions with J. Nitta, J. Fabian, K. Richter, M. H. Liu and S. Ilani are highly appreciated, and were indispensable for understanding some crucial issues.

---

[1] K. S. Novoselov, A. K. Geim, S. V. Morozov, D. Jiang, Y. Zhang, S. V. Dubonos, I. V. Grigorieva, and A. A. Firsov, *Science* **306**, 666 (2004); A. K. Geim and K. S. Novoselov *Nature Mater.* **6**, 183 (2007); A. K. Geim *Science* **324**, 1530 (2009).

[2] A. H. Castro Neto, F. Guinea, N. M. R. Peres, K. S. Novoselov, and A. K. Geim, *Rev. Mod. Phys.* **81**, 109 (2009).

[3] S. Das Sarma, Shaffique Adam, E. H. Hwang, and Enrico Rossi, *Rev. Mod. Phys.* **83**, 407 (2011).

[4] O. Klein, *Z. Phys.* **53**, 157 (1929); C. W. J. Beenakker, *Rev. Mod. Phys.* **80**, 1337 (2008).

[5] M. I. Katsnelson, K. S. Novoselov, and A. K. Geim, *Nature Physics* **2**, 620 (2006).

[6] T. Tudorovskiy, K. J. A. Reijnders and M. I. Katsnelson, *Phys. Scr.* **T146**, 014010 (2012).

[7] Vadim V. Cheianov and Vladimir I. Fal'ko, *Phys. Rev. B* **74**, 041403 (2006).

[8] Pierre E. Allain and J-N. Fuchs, *Eur. Phys. J. B* **83**, 301 (2011).

[9] T. Ando, and T. Nakanishi, *J. Phys. Soc. Jpn.* **67**, 1704 (1998).

[10] J. M. Pereira Jr., V. Molnar, F. M. Peeters, P. Vasilopoulos, *Phys. Rev. B* **74**, 045424 (2006).

[11] M. Barbier, P. Vasilopoulos, and F. M. Peeters, *Philosophical Transactions: Mathematical, Physical and Engineering Sciences* **368**, No. 193, 5499 (2010), arXiv:1101.4117.

[12] Y. Avishai and Y. B. Band, *Phys. Rev. B* **102**, 085435 (2020).

[13] H. D. Huertas, F. Guinea and A. Brataas, *Phys. Rev. B* **74**, 155426 (2006).

[14] H. Min, J.E. Hill, N.A. Shnitsyn, B.R. Sahu, L. Kleinman, and A.H. MacDonald, *Phys. Rev. B* **74**, 165310 (2006).

[15] Y. Yao, F. Ye, X. L. Qi, S. C. Zhang, and Z. Fang, *Phys. Rev. B* **75**, 041401(R) (2007).

[16] E. V. Castro, K. S. Novoselov, S. V. Morozov, N. M. R. Peres, J. M. B. L. dos Santos, J. Nilsson, F. Guinea, A. K. Geim, and A. H. Castro Neto, *Phys. Rev. Lett.* **99**, 216802 (2007).

[17] B. Trauzettel, D. V. Bulaev, D. Loss, and G. Burkard, *Nature Phys.* **3**, 192 (2007).

[18] N. Tombros, C. Jozsa, M. Popinciuc, H. T. Jonkman, and B. J. van Wees, *Nature* **448**, 571 (2007).

[19] N. Tombros *et al.*, *Phys. Rev. Lett.* **101**, 046601 (2008).

[20] S. Cho, Y. Chen, and M. S. Fuhrer, *Appl. Phys. Lett.* **91**, 123105 (2007).

[21] M. Zarea and N. Sandler, *Phys. Rev. B* **79**, 165442 (2009).

[22] E. I. Rashba, *Phys. Rev. B* **79**, 161409(R) (2009).

[23] M.-H. Liu and C.-R. Chang, *Phys. Rev. B* **80**, 241304(R) (2009).

[24] M. Gmitra, S. Konschuh, C. Ertler, C. Ambrosch-Draxl, and J. Fabian, *Phys. Rev. B* **80**, 235431 (2009).

[25] D. Bercioux and De Martino, *Phys. Rev. B* **81**, 165410 (2010).

[26] S. Konschuh, M. Gmitra, and J. Fabian, *Phys. Rev. B* **82**, 245412 (2010).

[27] F. Schwierz, *Nature Nanotechnol.* **5**, 487 (2010).

[28] W.-K. Tse, Z. Qiao, Y. Yao A. H. MacDonald, and Q. Niu, *Phys. Rev. B* **83**, 155447 (2011).

[29] S. Konschuh, *it Spin-Orbit Coupling Effects From Graphene To Graphite*, Ph.D. Thesis, Universität Regensburg, (2011).

[30] G. Miao, M. Münenberg, and J. S. Moodera, *Rep. Prog. Phys.* **74**, 036501 (2011).

[31] S. Jo, D. Ki, D. Jeong, H. Lee, and S. Kettemann, *Phys. Rev. B* **84**, 075453 (2011).

[32] J. F. Liu, B. K. S. Chan and J. Wang, *Nanotechnology*, **23**(9):095201 (2012).

[33] D. Marchenko, A. Varykhalov, M.R. Scholz, G. Bihlmayer, E.I. Rashba, A. Rybkin, A.M. Shikin and O. Rader, *Nature Communications* **3**, 1232 (2012).

[34] Ming-Hao Liu, Jan Bundesmann, and Klaus Richter, *Phys. Rev. B* **85**, 085406 (2012).

[35] A. K. Patra *et al.*, *Phys. Lett.* **101**, 162407 (2012).

[36] B. Dulbak *et al.*, *Nature Phys.* **8**, 557 (2012).

[37] P. J. Zomer *et al.*, *Phys. Rev. B* **86**, 161416(R) (2012).

[38] Q. Zhang, K. S. Chan, Z. Lin and J. F. Liu, *Phys. Lett. A* **377**, 632 (2013).

[39] L. Lenz, D. F. Urban and D. Bercioux, The European Physical Journal **B** **86**, 502 (2013).

[40] K. Shakouri, M. R. Masir, A. Jellal, E. B. Chouababi, and F. M. Peeters, Phys. Rev. **B** **88**, 115408 (2013).

[41] Z. Tang, E. Shikoh, H. Ago, K. Kawahara, Y. Ando, T. Shinjo, and M. Shiraishi, Phys. Rev. **B** **87**, 140401 (2013).

[42] W. Han, R. K. Kawakami, M. Gmitra and J. Fabian, Nature Nanotechnology **9**, 794 (2014).

[43] D. Kochan, M. Gmitra, and J. Fabian, Phys. Rev. Lett. **112**, 116602 (2014).

[44] *et al.*, Nature Phys. **10**, 857 (2014).

[45] M. Gmitra and J. Fabian, Phys. Rev. **B** **92**, 155403 (2015).

[46] A. C Ferrari *et al.*, Nanoscale **7**, 4598 (2015).

[47] S. Roch *et al.*, 2D Mater. **2**, 030202 (2015).

[48] H. Zhang, Z. Ma and J. F. Liu, Scientific Reports **4**, 6464 (2014).

[49] M. Dröegler *et al.*, Nano Lett. **16**, 3533 (2016).

[50] A. Avsar *et. al.*, NPG Asia Mater. **8**, 274 (2016).

[51] J. Ingla-Aynés, R. J. Meijerink, and B. J. van Wees, Nano Lett. **16**, 4825 (2016).

[52] B. Berche, F. Mireles, and E. Medina, Condensed Matter Physics **20**, 13702 (2017).

[53] X. Li, Z. Wu and J. Liu, Scientific Reports **7**, 6526 (2017).

[54] Xiaoyang Lin *et al.*, Phys. Rev. Appl. **8**, 034006 (2017).

[55] A. M. Afzal, K. H. Min, B. M. Ko and J. Eom, RSC Adv. **9**, 31797 (2019).

[56] S. Qi, Y. Han, F. Xu, X. Xu and Z. Qiao, Phys. Rev. **B** **99**, 195439 (2019).

[57] E. I. Rashba, Sov. Phys. Solid State **2**, 1109 (1960); Y. A. Bychkov and E. I. Rashba, JETP Lett. **39**, 78 (1984); H. A. Engel E. I. Rashba and B. I. Halperin, arXiv:cond-mat/0603306.

[58] J. Shi, P. Zhang, D. Xiao, and Q. Niu, Phys. Rev. Lett. **96**, 076604 (2006).

[59] A. Shnirman, *Geometric phases and spin-orbit effects*, Lecture 2 in Karlsruhe Institute of Technology.

[60] D. D. Awschalom, D. Loss, and N. Samarth, eds., *Semiconductor Spintronics and Quantum Computation* (Springer, Berlin, 2002).

[61] I. Zutic, J. Fabian, and S. Das Sarma, Rev. Mod. Phys. **76**, 323 (2004).

[62] N. Hatano, R. Shirasaki, H. Nakamura, Phys. Rev. **A** **75**, 032107 2007.

[63] S. Matityahu, Y. Utsumi, A. Aharony, O. Entin-Wohlman and C. A. Balseiro, Phys. Rev. **B** **93**, 075407 (2016).

[64] Y. Avishai and Y. B. Band, Phys. Rev. **B** **95**, 104429 (2017).